A Theoretical Study of the Wet Removal of Atmospheric Pollutants. Part III: The Uptake, Redistribution, and Deposition of (NH 4) 2 SO 4 Particles by a Convective Cloud Using a Two-Dimensional Cloud Dynamics Model

Andrea Flossmann, H. Pruppacher

▶ To cite this version:

Andrea Flossmann, H. Pruppacher. A Theoretical Study of the Wet Removal of Atmospheric Pollutants. Part III: The Uptake, Redistribution, and Deposition of (NH 4) 2 SO 4 Particles by a Convective Cloud Using a Two-Dimensional Cloud Dynamics Model. Journal of the Atmospheric Sciences, 1988, 45 (13), pp.1857 - 1871. 10.1175/1520-0469(1988)0452.0.CO;2 . hal-01905687

HAL Id: hal-01905687

https://uca.hal.science/hal-01905687v1

Submitted on 19 Oct 2021

VOL. 45, NO. 13 JOURNAL OF THE ATMOSPHERIC SCIENCES 1 JULY 1988

A Theoretical Study of the Wet Removal of Atmospheric Pollutants. Part III: The Uptake, Redistribution, and Deposition of $(NH_4)_2SO_4$ Particles by a Convective Cloud Using a Two-Dimensional Cloud Dynamics Model

A. I. FLOSSMANN AND H. R. PRUPPACHER

Institut fur Meteorologie, Johannes Gutenburg Universitat, Mainz, Federal Republic of Germany

(Manuscript received 24 March 1987, in final form 10 November 1987)

ABSTRACT

Our model for the scavenging of aerosol particles has been coupled with the two-dimensional form of the convective cloud model of Clark and Collaborators. The combined model was then used to simulate a convective warm cloud for the meteorological situation which existed at 1100 LST 12 July 1985 over Hawaii; assuming an aerosol size distribution of maritime number concentration and of mixed composition with $(NH_4)_2SO_4$ as the soluble compound. A shallow model cloud developed 26 min after the onset of convection leading to moderate rain which began after 45 min and ended after 60 min. Various parameters which characterize the dynamics and micophysics of the cloud, as well as the scavenging mechanism taking place inside and below the cloud were computed during the cloud development. The computation showed that: 1) the scavenged aerosol mass became redistributed inside the cloud water as the cloud grew, whereby the main aerosol mass scavenged always remained associated with the main water mass in the cloud; 2) in-cloud scavenging of aerosol particles was mainly controlled by nucleation while impaction scavenging played a negligible role; 3) below-cloud scavenging, which is caused by impaction scavenging, contributed only 5% to the overall particle scavenging and contributed about 40% to the aerosol mass in the rain on the ground; and 4) the sulfur concentrations inside the rain water were found to be reasonable as compared to observations available in literature, considering that the present model does not yet include the effects of SO_2 scavenging.

1. Introduction

Wet removal by clouds and precipitation plays an important role in the distribution and concentration of sulfur species in the atmosphere (Rodhe 1978, 1983). Numerous studies (e.g., Cogbill and Likens 1974; Galloway et al. 1976) have shown that sulfate, in turn, is a major component of the acidity of precipitation. For these reasons, the interaction of sulfur species with precipitating cloud systems is a topic of major importance in atmospheric chemistry.

Several field studies have addressed various aspects of this problem (e.g., Hegg and Hobbs 1982; Lazrus et al. 1983; Richards et al. 1983; Daum et al. 1983; Leaitch et al. 1983). However, the complexities of the processes involved suggest that field studies alone cannot completely resolve current uncertainties. Instead, a combination of models and field studies is likely the most expedient approach.

Several such modeling studies have been performed. Easter and Hobbs (1974) used an air parcel model to describe the motion of air along a streamline through a wave cloud, and the simultaneous production of cloud drops taking up SO_2 gas and converting it to sulfate. The purpose of this model was to account for the increased CCN concentration found on the downstream side of wave clouds. Ohta et al. (1981) used a simple parcel model to describe air which ascended along the side of a mountain slope producing cloud drops which acquire salt particles by nucleation and pollutant gases by diffusion. Walcek and Taylor (1986) formulated a one-dimensional, semi-empirical top-down entraining model based on the observation of Paluch (1979), to describe the vertical variation of the cloud liquid water content and the uptake of soluble aerosol particles and numerous pollutant gases by the cloud water, allowing the collected compounds to be oxidized and acid to be formed. Similarly, Fischer (1982) used a one-dimensional model with Kessler-type parameterization of the cloud microphysics to determine the uptake of SO_2 by the cloud water and the transformation of the uptaken SO_2 into sulfate. Scott (1978, 1982) described one-dimensional convective storm models with parameterized microphysics, sulfate scavenging and in-solution production by uptaken SO_2 gas. The latter of these models was employed as an interpretative tool for analyzing field data.

Hales (1982) constructed a highly simplified one-dimensional, time dependent storm model capable of predicting the precipitation scavenging of reactive and nonreactive pollutants and elucidating observed sulfate

---

Corresponding author address: Dr. Hans Pruppacher, Institut fur Meteorologie, Johannes Gutenburg Universitat, D-6500 Mainz, Postfach 39 80, Federal Republic of Germany.

deposition patterns and concentrations. The model of Scott (1982) was subsequently extended to two dimensions by Easter and Hales (1983). The microphysics parameterization was similar to that of Scott following the water mass in four categories: water vapor, cloud water, rain water and snow. Aerosol particle scavenging was assumed to occur solely by nucleation; SO_2 gas was assumed to be taken up by the cloud water through a diffusion process under equilibrium. The uptaken SO_2 was allowed to be oxidized to sulfate using prescribed oxidation rate constants. A model conceptually similar to that of Easter and Hales was formulated by Hegg et al. (1984) employing the dynamic framework of the warm frontal rainband model described by Rutledge and Hobbs (1983).

Sarma (1983) modified the two-dimensional, time-dependent cloud model of Orville (1965) to include parameterizations of the aqueous phase oxidation of sulfur dioxide by ozone, in order to examine the distribution of acidity in cumulus clouds caused by in-solution sulfate production. In the model, equilibrium was assumed to exist between SO_2 and the cloud water. Tremblay and Leighton (1984) used a one-dimensional version of the three-dimensional dynamic model of Yau (1980) to describe the evolution of sulfur dioxide, sulfate and ammonia within rain systems. They used a Kessler-type bulk parameterization for the condensation-evaporation and cloud drop growth processes and assumed the pollutant gases were in equilibrium with the cloud water at all times. Molenkamp (1983) formulated a two-dimensional axisymmetric Lagrangian cloud model involving scale dependent diffusion with transport along a trajectory deduced from measured winds. A Kessler-type parameterization was used for describing the cloud microphysics with the addition of a snow phase based on observed snowflake size spectra. A specific fraction of aerosol material, chemically not characterized and in concentration of arbitrary units, was assumed to be incorporated into the cloud water. The rate of attachment of aerosol particles to the cloud water was computed via semi-empirical efficiency functions.

Finally, Chaumerliac et al. (1983) formulated a three-dimensional mesoscale model with the capability to simulate orographically forced clouds and precipitation, as well as interactions of aerosol particles with the clouds and precipitation. In this model, the microphysical processes were taken into account through prescribed log-normal distributions of cloud drops, rain drops and aerosol particles. Although Chaumerliac et al. use two parameters for each type of hydrometeor (which is one more than most others in the literature), they are unable to correctly compute nucleation scavenging. This is because they use a simple exponential relation between the number concentration of CCN and the supersaturation, which does not allow for CCN entrainment into the cloud.

The above models give insight into the wet deposition of atmospheric pollutants, but they lack realism from a cloud *microphysics* point of view in that the microphysical processes were considerably simplified by bulk parameterizations, and, in some cases, the clouds were not allowed to precipitate. Other models lack realism, from a *cloud dynamics* point of view, because the dynamics behavior of the cloud was idealized by a parcel or one-dimensional treatment. Many also lack realism in their *treatment of the scavenging mechanism,* in that the effects of nucleation scavenging were not considered or the drops were assumed to be in gas equilibrium at all times.

2. Motivation and general approach

In an attempt to remedy some of the inadequacies of past scavenging models and to gain a more detailed insight into the interplay between the dynamics of a cloud and the microphysical processes which determine the scavenging of aerosol particles and gases, we formulated a cloud microphysics model for the scavenging of aerosol particles and gases which could be incorporated into the framework of any dynamic model.

In the first two articles of a series, we checked the performance of the scavenging model by linking it to a simple entraining air parcel model. This configuration was tested for the case of a warm cloud and for aerosol particles of various compositions by Flossmann et al. (1985), and for the case of a warm cloud with ammonium sulfate particles simultaneously present with SO_2 gas by Flossmann et al. (1987).

It is obvious that entraining air parcels reflect the dynamics of a convective cloud only in a limited way. Therefore, the results derived from using an entraining air parcel model had to be checked by a more realistic dynamic model. It is well known that the dynamics of a cloud substantially controls the microphysical processes (condensation–evaporation, collisional growth), and consequently the scavenging processes. In particular, it was necessary to investigate for aerosol particle scavenging: 1) the *importance of nucleation scavenging* inside a cloud; 2) the *redistribution of the scavenged material* inside the cloud water, both predicted by our air parcel model; and 3) the *contribution of below-cloud scavenging* to total scavenging, which could not be studied by the air parcel model.

Since present three-dimensional models only allowed us to include the cloud microphysical processes in a highly parameterized fashion (which we precisely wanted to avoid) we decided to link our scavenging model to a two-dimensional dynamic model for a convective cloud. The detailed formulation of the microphysical processes allows prediction of the time and space variation of the cloud microstructure (drop size distribution, aerosol particle size distribution, liquid water and aerosol particle content) at each grid point of the model.

With the two-dimensional model we decided, as a first step, to focus on obtaining some answers to the three problem areas listed above, particularly because our present two-dimensional model does not yet include gas scavenging. The decision was made to postpone modeling the local chemistry of a given geographic location. However, even for this general purpose it was necessary to choose some reasonable atmospheric situation as an initial condition for running the model. We chose to study at first warm clouds, whose tops stay below the 0°C level, in order to avoid the complications which arise from introducing an ice phase into the model. Therefore, the atmospheric sounding of 1100 LST 12 July 1985 over Hilo, Hawaii was selected. Aerosol particles with a maritime number concentration (see section 4) and a mixed composition were chosen, with $(NH_4)_2SO_4$ as the water soluble compound. The total mass mixing ratio of the aerosol mass was decided to be 28.65 μg m^{-3}, of which 2.08 μg m^{-3} was sulfate (equivalent to 0.69 μg m^{-3} sulfur) (see section 4), in order to be qualitatively consistent with the field measurements of Darzi and Winchester (1982). During the special situation of East Asian dust storm episodes over Hawaii, Darzi and Winchester found aersol particle mixing ratios in excess of 20 μg m^{-3} with median sulfur concentrations of 0.30 μg m^{-3} and maximum sulfur concentrations of 6.6 μg m^{-3}.

This special Hawaiian situation, with aerosol particles composed of considerable amounts of water insoluble material, will help in future comparisons of the results derived from our maritime warm model cloud and the results of our model applied to a continental cloud with the ice phase included. For the latter case it is necessary to assume aerosol particles with some water insoluble portion. By using the same mass fraction of sulfate to total aerosol mass, we will then be able to eliminate the aerosol particle composition as a factor in the scavenging. This will allow us to attribute the differences between a maritime and a continental cloud to the aerosol particle number distribution, the presence or absence of an ice phase, and the dynamic characteristics alone.

3. The present model

The basic dynamic framework employed in this study is a two-dimensional slab-symmetric version of the three-dimensional model, which has been described in detail, e.g., by Clark (1977, 1979), Clark and Gall (1982), Clark and Farley (1984), and Hall (1980), whose formalism shall be used below.

The model utilizes the anelastic form of the equations of motion, continuity, and the first law of thermodynamics. The anelastic framework permits the thermodynamic variables to be cast into a perturbation form. The form taken is

$$\begin{aligned}
\theta &= \bar{\theta}(z) + \tilde{\theta}(z) + \theta'(x, z, t) = \bar{\theta}(z)(1 + \theta^*) \\
T &= \bar{T}(z) + \tilde{T}(z) + T'(x, z, t) = \bar{T}(z)(1 + T^*) \\
p &= \bar{p}(z) + \tilde{p}(z) + p'(x, z, t) = \bar{p}(z)(1 + p^*) \\
\rho &= \bar{\rho}(z) + \tilde{\rho}(z) + \rho'(x, z, t) = \bar{\rho}(z)(1 + \rho^*) \\
w_v &= \tilde{w}_v(z) + w_v'(x, z, t) \qquad (1)
\end{aligned}$$

where z is the Cartesian coordinate in the vertical direction. The potential temperature, temperature, pressure, density of dry air, and water vapor mixing ratio are θ, T, p, ρ and w_v, respectively. The terms in (1) with overbars represent the atmospheric conditions for an idealized atmosphere with constant stability Γ (see Clark and Farley 1984). This is the atmosphere in which a linear perturbation theory is applied. The terms in (1) with tildes represent the differences between the actual hydrostatically-balanced environmental sounding and the constant stability atmosphere. The x and t represent the horizontal Cartesian coordinate and time. The terms in (1) with the asterisk represent normalized deviations from the chosen idealized constant stability environment. The overbar terms are taken as

$$\begin{aligned}
\bar{\theta}(z) &= \theta_0 \exp(\Gamma z) \\
\bar{T}(z) &= \theta_0 \exp(\Gamma z)\left\{1 - \frac{g}{c_p \theta_0 \Gamma}[1 - \exp(-\Gamma z)]\right\} \\
\bar{p}(z) &= p_0\left\{1 - \frac{g}{c_p \theta_0 \Gamma}[1 - \exp(-\Gamma z)]\right\}^{1/\kappa} \\
\bar{\rho}(z) &= \rho_0 \exp(-\Gamma z)\left\{1 - \frac{g}{c_p \theta_0 \Gamma} \times [1 - \exp(-\Gamma z)]\right\}^{(1/\kappa)-1} \qquad (2)
\end{aligned}$$

where θ_0, p_0 and ρ_0 represent the environmental potential temperature, pressure and density at $z = 0$ of the model. Here c_p is the specific heat of the air at constant pressure, $\kappa = R/c_p$ where R is the gas constant, and g is the acceleration of gravity.

In Cartesian coordinates the horizontal and vertical momentum equations are

$$\bar{\rho}\frac{du}{dt} = -\frac{\partial p'}{\partial x} + \frac{\partial \tau_{11}}{\partial x} + \frac{\partial \tau_{13}}{\partial z} \qquad (3)$$

$$\bar{\rho}\frac{dw}{dt} = -\frac{\partial p'}{\partial z} + \bar{\rho} g\left[\frac{\theta'}{\bar{\theta}} + 0.608 w_v' - \frac{c_v p'}{c_p \bar{p}} - w_L\right] + \frac{\partial \tau_{31}}{\partial x} + \frac{\partial \tau_{33}}{\partial z} \qquad (4)$$

where u = horizontal velocity, w = vertical velocity, τ_{ij} = Reynolds stress tensor, w_L = liquid water mixing ratio.

The anelastic form of the continuity equation is expressed as

$$\frac{\partial}{\partial x}(\bar{\rho} u) + \frac{\partial}{\partial z}(\bar{\rho} w) = 0 \qquad (5)$$

and the first law of thermodynamics is expressed by

$$\bar{\rho}\frac{d\theta^*}{dt} = \frac{\bar{\rho}L_v}{c_p\bar{T}}C_{Ph} + \nabla\cdot(\bar{\rho}K_m\nabla\theta^*) \quad (6)$$

where: L_v is latent heat of evaporation, K_m the eddy mixing coefficient and C_{Ph} the change of water vapor mixing ratio due to condensation or evaporation.

The stress tensor is taken proportional to the deformation D_{ij} according to the first-order theory of Smagorinsky (1963) and Lilly (1962) where

$$\tau_{ij} = \bar{\rho}K_m D_{ij} \quad (7)$$

and the deformation tensor D_{ij} and the eddy mixing coefficient K_m are expressed as

$$D_{ij} = \frac{\partial u_i}{\partial x_j} + \frac{\partial u_j}{\partial x_i} - \frac{2}{3}\delta_{ij}\frac{\partial u_k}{\partial x_k} \quad (8)$$

$$K_m = \begin{cases} \frac{(C\Delta)^2}{\sqrt{2}}|\mathrm{Def}|(1 - \mathrm{Ri})^{1/2}, & \mathrm{Ri} < 1 \\ 0, & \mathrm{Ri} \geqslant 1 \end{cases} \quad (9)$$

where Def is the total deformation in two dimensions and Ri is the local Richardson number, with $C = 0.2$, and

$$\mathrm{Def} = \frac{1}{2}[(D_{11}^2 + D_{33}^2) + D_{13}^2]^{1/2} \quad (10)$$

$$\mathrm{Ri} = g\frac{\partial}{\partial z}[\theta^* + 0.608w_v - w_L]\,\mathrm{Def}^{-2}. \quad (11)$$

The same eddy mixing coefficient used for momentum is applied to the eddy mixing of heat and moisture, i.e., an eddy Prandtl number of unity is assumed. Also, the effective grid scale, Δ, is

$$\Delta = (\Delta x\Delta z)^{1/2} \quad (12)$$

where Δx and Δz are the model grid spacing for the horizontal and vertical directions, respectively.

The continuity equation for water vapor is written as

$$\bar{\rho}\frac{dw_v}{dt} = -C_{Ph} + \nabla\cdot(\bar{\rho}K_m\nabla w_v). \quad (13)$$

The above framework for modeling the dynamics of convective clouds was coupled with our model for the scavenging of aerosol particles, where, following Flossmann et al. (1985)

$$C_{Ph} = \bar{\rho}\frac{dw_L}{dt} - \nabla\cdot(\bar{\rho}K_m\nabla w_L) \quad (14)$$

with w_L given by Eq. (31) in Flossmann et al. (1985). The supersaturation, as determined by the dynamics and microphysics of the cloud was computed following Hall (1980). For details see Flossmann (1987).

The time rate of change of the cloud drop number density distribution function f_d is given by the relation

$$\frac{\partial f_d(m)}{\partial t} = -\nabla\cdot[\mathbf{v}f_d(m)] + \nabla\cdot[K_m\nabla f_d(m)] + \frac{\partial}{\partial z} \times [V_\infty(m)f_d(m)] + \left.\frac{\partial f_d(m)}{\partial t}\right|_{\mathrm{act}} + \left.\frac{\partial f_d(m)}{\partial t}\right|_{\mathrm{con/eva}} + \left.\frac{\partial f_d(m)}{\partial t}\right|_{\mathrm{AP,coll}} + \left.\frac{\partial f_d(m)}{\partial t}\right|_{d,\mathrm{coal}} + \left.\frac{\partial f_d(m)}{\partial t}\right|_{d,\mathrm{break}}. \quad (15)$$

The time rate of change of the number density distribution function for aerosol particles remaining in the air, $f_{\mathrm{AP}a}$, is given by

$$\frac{\partial f_{\mathrm{AP}a}(m_{\mathrm{AP}})}{\partial t} = -\nabla\cdot[\mathbf{v}f_{\mathrm{AP}a}(m_{\mathrm{AP}})] + \nabla\cdot[K_m\nabla f_{\mathrm{AP}a}(m_{\mathrm{AP}})] + \left.\frac{\partial f_{\mathrm{AP}a}(m_{\mathrm{AP}})}{\partial t}\right|_{\mathrm{act}} + \left.\frac{\partial f_{\mathrm{AP}a}(m_{\mathrm{AP}})}{\partial t}\right|_{\mathrm{con/eva}} + \left.\frac{\partial f_{\mathrm{AP}a}(m_{\mathrm{AP}})}{\partial t}\right|_{\mathrm{AP,coll}}. \quad (16)$$

The time rate of change of the mass density distribution function of aerosol particles in the drops, $g_{\mathrm{AP}d}$, is given by

$$\frac{\partial g_{\mathrm{AP}a}(m_{\mathrm{AP}})}{\partial t} = -\nabla\cdot[\mathbf{v}g_{\mathrm{AP}a}(m_{\mathrm{AP}})] + \nabla\cdot[K_m\nabla g_{\mathrm{AP}a}(m_{\mathrm{AP}})] + \left.\frac{\partial g_{\mathrm{AP}a}(m_{\mathrm{AP}})}{\partial t}\right|_{\mathrm{act}} + \left.\frac{\partial g_{\mathrm{AP}d}(m)}{\partial t}\right|_{\mathrm{con/eva}} + \left.\frac{\partial g_{\mathrm{AP}d}(m)}{\partial t}\right|_{\mathrm{AP,coll}} + \left.\frac{\partial g_{\mathrm{AP}d}(m)}{\partial t}\right|_{d,\mathrm{coal}} + \left.\frac{\partial g_{\mathrm{AP}d}(m)}{\partial t}\right|_{d,\mathrm{break}}, \quad (17)$$

and the time rate of change of the mass density distribution function for the aerosol particles remaining in the air, $g_{\mathrm{AP}a}$, is given by

$$\frac{\partial g_{\mathrm{AP}a}(m_{\mathrm{AP}})}{\partial t} = -\nabla\cdot[\mathbf{v}g_{\mathrm{AP}a}(m_{\mathrm{AP}})] + \nabla \times [K_m\nabla g_{\mathrm{AP}a}(m_{\mathrm{AP}})] + \left.\frac{\partial g_{\mathrm{AP}a}(m_{\mathrm{AP}})}{\partial t}\right|_{\mathrm{act}} + \left.\frac{\partial g_{\mathrm{AP}a}(m_{\mathrm{AP}})}{\partial t}\right|_{\mathrm{con/eva}} + \left.\frac{\partial g_{\mathrm{AP}a}(m_{\mathrm{AP}})}{\partial t}\right|_{\mathrm{AP,coll}} \quad (18)$$

where m is drop mass, m_{AP} the aerosol particle mass, $\mathbf{v}$ the velocity field of air, $g_w(m)$ the cloud drop mass distribution function $\{= m[1 - Q_{\mathrm{AP}d}(m)]f_d(m)\}$; ψ is time rate of change of the functions f_d, $g_{\mathrm{AP}d}$, $f_{\mathrm{AP}a}$, $g_{\mathrm{AP}a}$; $\psi|_{\mathrm{act}}$ is change due to activation of aerosol particles to drops, $\psi|_{\mathrm{con/eva}}$ the change due to condensation and/or evaporation of drops, $\psi|_{\mathrm{AP,coll}}$ the change due to aerosol particle collection, $\psi|_{d,\mathrm{coal}}$ the change due to collision and coalescence of drops, $\psi|_{d,\mathrm{break}}$ the change due to drop break up, $Q_{\mathrm{AP}a}(m_{\mathrm{AP}})$ the aerosol mass mixing ratio distribution function $\{=g_{\mathrm{AP}a}(m_{\mathrm{AP}})/[m_{\mathrm{AP}}f_{\mathrm{AP}a}(m_{\mathrm{AP}})]\}$ and $Q_{\mathrm{AP}d}(m)$ is aerosol mass mixing ratio distribution function $\{=g_{\mathrm{AP}d}(m)/[mf_d(m)]\}$.

The first three terms in Eqs. (15) and (17) and the first two terms in Eqs. (16) and (18) were evaluated from the above described dynamic framework of the two dimensional cloud dynamics model. The remaining microphysical terms were evaluated from the equations given and discussed in detail by Flossmann et al. (1985).

4. Initial conditions and description of heating source

The present model was initialized with a warm cloud sounding taken at Hilo, Hawaii at 1100 LST 12 July 1985 (see Fig. 1). The total number concentration of the aerosol particles was chosen to be 590 cm^{-3}, and the initial size distribution function for the dry particles was given by a modified gamma function

$$f_{\mathrm{AP}a}(\ln r) = Ar^{\alpha+1}\exp(-Br^{\gamma}) \qquad (19)$$

with $A = 2.5 \times 10^6$ cm^{-3} μm^{-2}, $B = 15$ μm$^{-0.5}$, $\alpha = 1$, $\gamma = 0.5$. The total mass mixing ratio of the aerosol particles, $w_{\mathrm{AP}a}$, was 28.65 μg m^{-3}. All aerosol particles were assumed to be of uniform composition, consisting of 10% ammonium sulfate and 90% insoluble silicate. Therefore, the mass mixing ratio for $(NH_4)_2SO_4$ was 2.87 μg m^{-3}, equivalent to 2.08 μg m^{-3} SO_4 or 0.69 μg m^{-3} sulfur, consistent with the field measurements of Darzi and Winchester (1982). The specific gravity of these aerosol particles was assumed to be 2.0 g cm^{-3}. For a discussion of the values given above see section 2. From the size distribution of the dry aerosol particles (Eq. 19), we computed the initial size distribution for the moist aerosol particles by allowing the dry particles to grow to their equilibrium size at the local relative humidity.

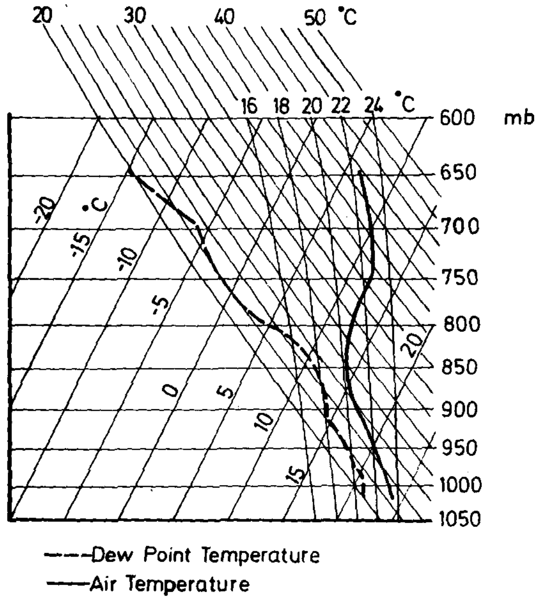

FIG. 1. Sounding for 1100 LST 12 July 1985, at Hilo, Hawaii.

The present model covered a domain of 10 km in the vertical and 20 km in the horizontal. The grid spacings were $\Delta z = 200$ m and $\Delta x = 400$ m, and the time step was $\Delta t = 5$ sec.

The dynamic model of Clark and collaborators, which we used for our model study, is driven by a sensible and latent heat flux from the surface as formulated by Clark and Gall (1982) and by a parameterized version of the detailed calculations of Smolarkiewicz and Clark (1985). In their studies, the fluxes were assumed to be proportional to the incoming shortwave solar flux S, so that

$$S = S_0 \cos Z \qquad (20)$$

where S_0 is the solar constant taken as 1395 W m^{-2}, and Z is the sun's zenith angle given by

$$\cos Z = \sin\varphi \sin\delta + \cos\varphi \cos\delta \cos\phi_r \qquad (21)$$

where φ is the geographic latitude, δ is the sun's declination angle,

$$\delta = \frac{23.45}{180}\pi \cos\left[\frac{2\pi(n_d - 172)}{365}\right], \qquad (22)$$

n_d is the number of the chosen day of the year, ϕ_r is the solar hour angle

$$\phi_r = \frac{\pi(12 - h_d)}{12} \qquad (23)$$

and h_d is the hour of the day.

The average surface sensible heat flux P_H was assumed to be 58%, and the latent heat flux P_Q to be 2% of the incoming solar flux. These fluxes are assumed to consist of a background heat flux and a Gaussian perturbation fraction. The surface sensible heat flux is thus represented by

$$H = \frac{P_H S}{1 + \dfrac{\alpha_H\sqrt{2\pi}}{6}}\left[1 + \alpha_H \exp\left(\frac{-(x - x_0)^2}{2\sigma_H^2}\right)\right] \qquad (24)$$

and the surface latent heat flux is

$$Q = \frac{P_Q S}{1 + \dfrac{\alpha_Q\sqrt{2\pi}}{6}}\left[1 + \alpha_Q \exp\left(\frac{-(x - x_0)^2}{2\sigma_Q^2}\right)\right], \qquad (25)$$

with

$$\alpha_H = \frac{6\beta_H}{\sqrt{2\pi}(1 - \beta_H)} \qquad (26)$$

$$\alpha_Q = \frac{6\beta_Q}{\sqrt{2\pi}(1 - \beta_Q)} \qquad (27)$$

where it was assumed that the fraction of the total energy which goes into the Gaussian perturbation of the sensible heat flux was $\beta_H = 50\%$ and the fraction that goes into the Gaussian perturbation of the latent heat flux was $\beta_Q = 0.1\%$. We assumed that the half-width of the Gaussian perturbation was $\sigma_H = 3600$ m and $\sigma_Q = 3600$ m. The coordinate x_0 locates the middle of the domain where the cloud was forced to develop. These heat and moisture sources were assumed to have their maximum value at the ground and attenuate exponentially with height so that at 150 m they had decreased in strength to $1/e$ of their surface value.

The complete composite model was evaluated on the CRAY-1A at the National Center for Atmospheric Research in Boulder, Colorado. The model run required 5 hours of computer time.

TABLE 1. Pertinent extreme values of cloud characteristics.

	Time (min)			
	20	30	45	60
$RH_{\max}$ (%)	91.4	102.4	102.0	100.9
$w_{\max}$ (m s^{-1})	0.28	9.45	8.20	6.20
$w_{L,\max}$ (g kg^{-1})	2.15×10^{-5}	0.75	1.64	2.16
$w_{APd,\max}$ (g kg^{-1})	0	2.3×10^{-5}	2.63×10^{-5}	2.76×10^{-5}
$w_{APa,\min}$ (g kg^{-1})	2.1×10^{-5}	6.0×10^{-8}	2.0×10^{-7}	3.3×10^{-7}

5. Results and discussion

The results of our study are summarized in Figs. 2–13, and Tables 1–3. In Figs. 2–10 vertical cross sections of the following quantities are plotted at 20, 30, 45, and 60 minutes: potential temperature, θ, relative humidity, RH, horizontal velocity, u, vertical velocity, w, mass distribution function of the aerosol particles in the air, g_{APa}, mass distribution function of the aerosol particles in the cloud water, g_{APd}, cloud drop mass distribution function, g_w, liquid water content w_L, mass mixing ratio of aerosol particles in the air, w_{APa}, and mass mixing ratio of the aerosol particles in the cloud water, w_{APd}. In the following, we shall discuss the behavior of these functions at specific times after cloud initiation.

At t = 20 minutes. Figure 2 shows the distribution of (a) θ, (b) RH, (c) u, and (d) w. Note the warming of the air near the ground due to the sensible heat flux, the rise of relative humidity between 500 and 1000 m with a maximum of 91.4% (see Table 1), the convergence–divergence system set up in the flow near the ground, the rising air at the domain center with a maximum velocity of 0.28 m s^{-1} (see Table 1), and the downdraft at the domain's sides. In Fig. 3 we have plotted (a) g_{APa} and (b) w_L. Note from Fig. 3a that the size distribution of the aerosol particles is still uniform at all grid points, with the exception of a slight shift of the aerosol size spectrum towards larger sizes in the center of the domain due to the uptake of moisture by particles. This is also reflected by the behavior of w_L, which rises to a maximum of 2.15×10^{-5} g kg^{-1} (see Table 1).

At t = 30 minutes. Figure 4 shows the distribution of (a) θ, (b) RH, (c) u, and (d) w. Note that the warm-

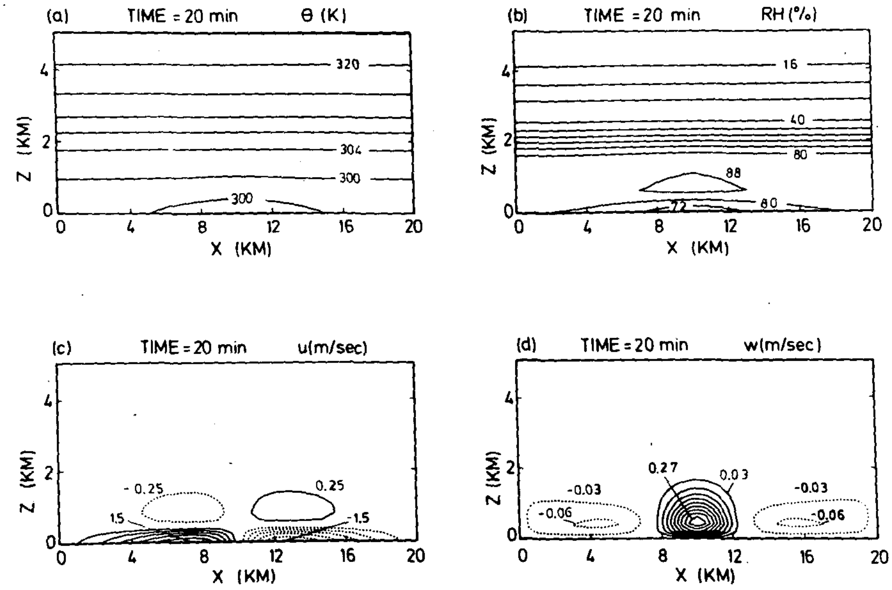

FIG. 2. Distribution of (a) θ, (b) RH, (c) u, and (d) w inside domain at $t = 20$ min; $\Delta\theta = 4°$K, $\Delta RH = 8\%$, $\Delta u = 0.25$ m s^{-1}, $\Delta w = 0.03$ m s^{-1}.

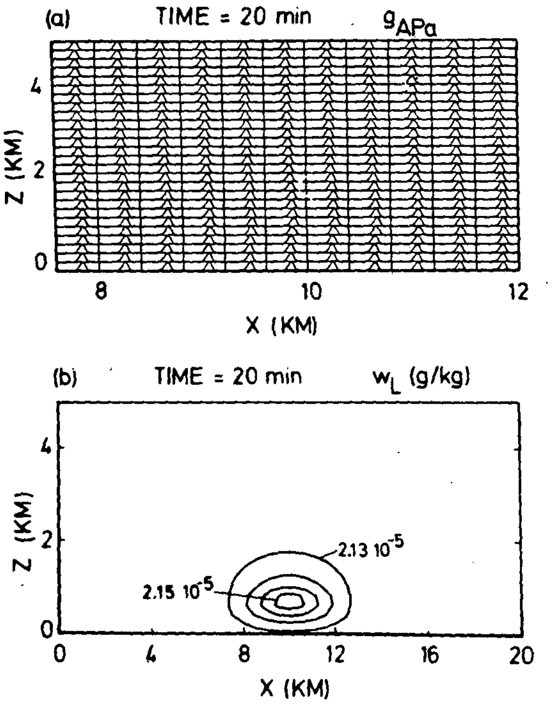

FIG. 3. Distribution of g_{APa} and w_L inside domain at $t = 20$ min; $\Delta w_L = 6.66 \times 10^{-8}$ g kg^{-1}; on the left-hand side and right-hand side of each box $r = 10^{-3}$ and 10 μm, respectively.

ing of the air due to heat flux from the ground has increased and so has the convergence–divergence pattern and the updraft with a maximum of 9.45 m s^{-1} (see Table 1). The relative humidity has increased to a local maximum of 102.4%, equivalent to a supersaturation of 2.4%. In Fig. 5a and 5b, notice that a cloud has formed and has a maximum liquid water content w_L of 0.75 g kg^{-1}. Most of the liquid water is in drops of radius smaller than 30 μm. In Fig. 5c the mass mixing ratio, w_{APd}, of the aerosol particle material inside the cloud water is displayed. Notice that the main aerosol mass is associated with the main water mass inside the cloud. Correspondingly, Fig. 5d illustrates the "consumption pattern" of aerosol particles by showing that the mass mixing ratio of aerosol particles, w_{APa}, left as drop–interstitial aerosol is greatly reduced inside the cloud. Such an interstitial aerosol has been found in field studies by various authors, e.g., Radke (1983). Figure 6a shows how the liquid water inside the cloud is distributed over the various drop size categories. The drop mass distribution function g_w demonstrates that most of the liquid water is still contained in the small cloud drop size categories and no precipitation size drops have developed yet. Comparing the mass density distribution function of aerosol particles in the drops, g_{APd}, in Fig. 6b, with Fig. 6a, shows that the main aerosol mass is associated with the main water mass inside the cloud. The changes in the size distribution of aerosol particles in the air, g_{APa}, caused by nucleation of aerosol particles to drops, is displayed in Fig. 6c. Inside the cloud region, all large particles have disappeared due to consumption by nucleation and only particles much smaller than 0.1 μm are left in the air. Also note the shift of the aerosol particle spectrum towards larger sizes near the cloud edges due to "wet" aerosol particles. The double maximum in the aerosol particle size spectrum near the cloud edges is due to entrainment of large particles into size categories emptied by previous nucleation. These particles are now additionally available for nucleation in the next time step.

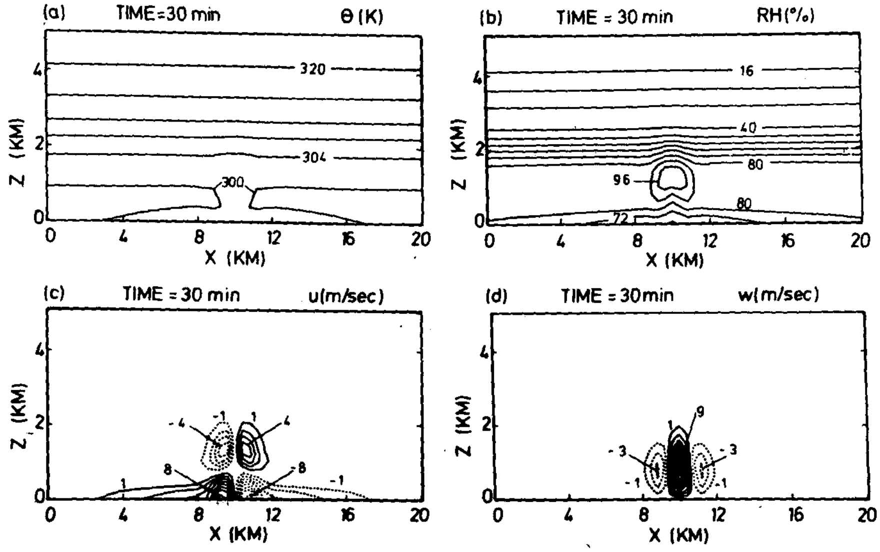

FIG. 4. Distribution of (a) θ, (b) RH, (c) u, and (d) w inside domain at $t = 30$ min; $\Delta\theta = 4$°K, $\Delta RH = 8\%$, $\Delta u = 1$ m s^{-1}, $\Delta w = 1$ m s^{-1}.

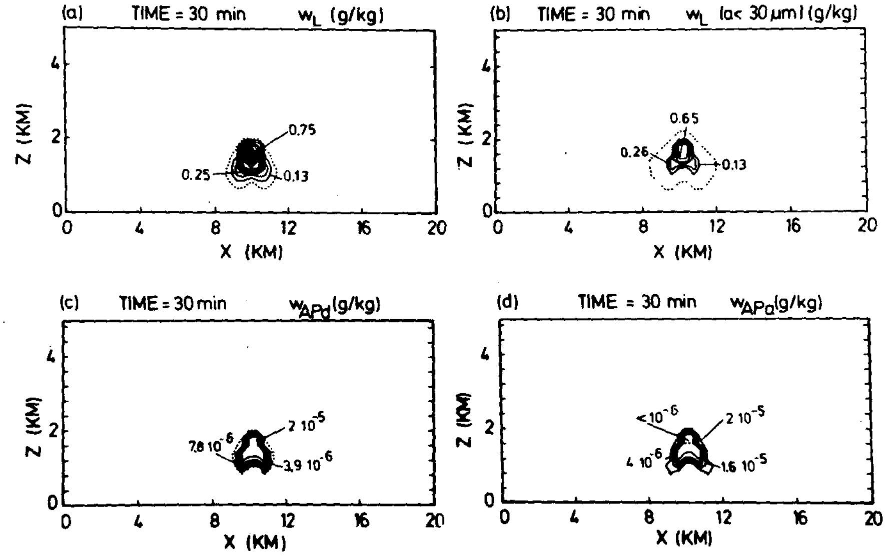

FIG. 5. Distribution of (a) w_L, (b) w_L for drops of $a < 30\ \mu$m, (c) w_{APd}, and (d) w_{APa} inside domain at t = 30 min; $\Delta w_L = 0.125$ g kg^{-1}, Δw_L ($a < 30\ \mu$m) = 0.13 g kg^{-1}, $\Delta w_{APd} = 3.9 \times 10^{-6}$ g kg^{-1}, $\Delta w_{APa} = 4 \times 10^{-6}$ g kg^{-1}.

At t = 45 minutes. Figure 7 shows the distribution of (a) θ, (b) RH, (c) u, and (d) w. The thermal disturbance has now reached 6 km, and the moisture field has split into five supersaturated regions with a maximum supersaturation of 2.0% associated with an updraft of 8.2 m s^{-1} (see Table 1). The splitting of the supersaturated region is the result of downdrafts (see Fig. 7d) which develop near the cloud edges and bring down drier air. The convergence–divergence flow pattern (see Fig. 7c) has become more complex, has widened, and extends to higher levels. Fig. 8a and 8b demonstrate that, at 45 minutes, liquid water is falling to the ground as rain. Inside the cloud, two maxima of liquid water have formed, the largest value reaching 1.64 g kg^{-1} (see Table 1). Figure 8c shows that the distribution of the mass mixing ratio for aerosol particles inside the cloud and rain water, w_{APd}, closely follows the distribution of the liquid water content, w_L, indicating again that the main aerosol mass is always associated with the main water mass. The "consumption pattern" of the aerosol particles is reflected by Fig. 8d which shows the mass mixing ratio of aerosol particles, w_{APa}, left as interstitial aerosol inside the cloud. In Fig. 9a the drop mass distribution function, g_w, is plotted at various locations inside the cloud–precipitation domain. The drops have now grown considerably compared to Fig. 6a at 30 minutes and have reached millimeter size in the low portion of the domain. Comparing the mass density distribution function of aerosol particles in the drops, g_{APd} (Fig. 9b) with g_w (Fig. 9a) shows again that the main aerosol mass is associated with the main water mass, even when most of the water is in precipitating drops.

At t = 60 minutes. Figures 10a and 10b show the liquid water content pattern of a slowly deteriorating precipitation system. The main cloud body has now split up into three distinct regions, and the liquid water associated with the precipitation is significantly reduced, i.e. precipitation from the cloud is stopping. Figures 10c and 10d demonstrate, again, how closely the distribution of the liquid water is reflected by the pattern of w_{APd} and w_{APa}, i.e., how closely the maxima of the liquid water are associated with the maxima of w_{APd} and the minima of w_{APa}.

It is quite instructive to compare the water budget of the cloud with the aerosol particle budget. For that purpose, Fig. 11 shows, as a function of time, the cumulative condensed water mass (curve 1), the total water mass as drops in air (curve 2), and the cumulative water mass which reached the ground as rain (curve 3). A cloud began to develop about 26 minutes after the heating began, and precipitation started reaching the ground after about 43 minutes. A close look at curve 1 shows that about one-half of the condensation occurs after the precipitation starts near 43 minutes. From curve 2 we notice that the total airborne water mass decreases by nearly one-half from the time it reached its maximum near 37 minutes till the end of simulation time. The decrease of this curve right after its maximum is due to evaporation of drops. The subsequent decrease is due to the fallout of rain. The sum of curves 2 and 3 gives the total liquid water in the domain, and the difference between this sum and curve 1 is due to the loss of water vapor by evaporation. In Fig. 12 the total aerosol mass in the air of the computational domain (curve 4), the cumulative mass of aerosol scavenged by nucleation (curve 5), the total

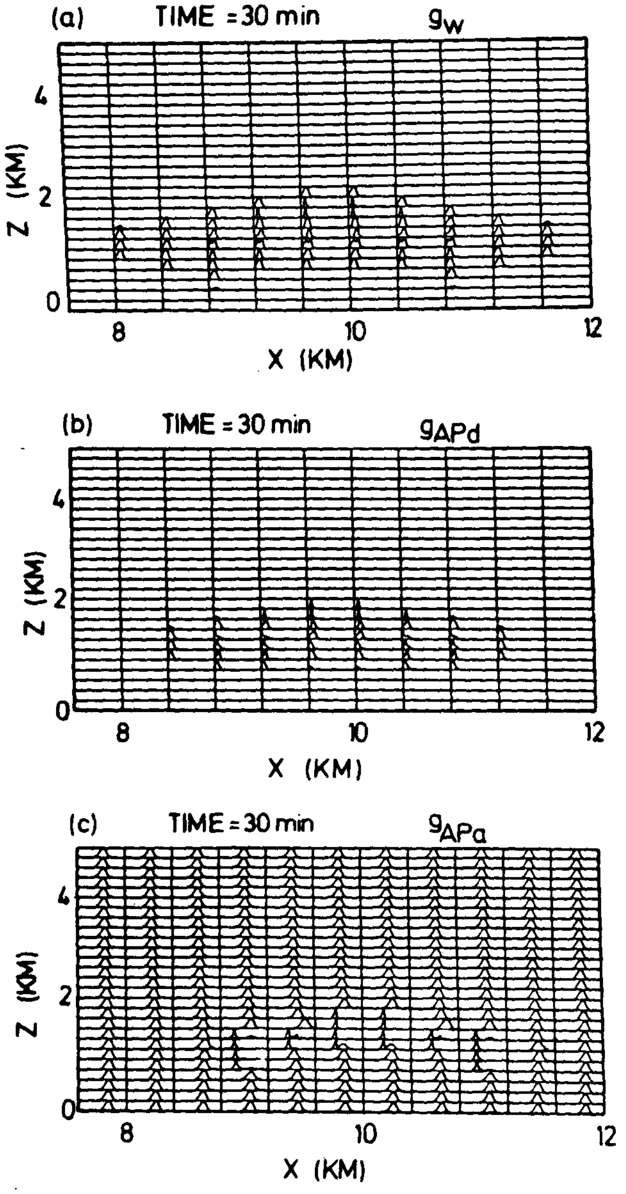

FIG. 6. Distribution of (a) g_w, (b) g_{APd}, (c) g_{APa} inside domain at $t = 30$ minutes; on the left-hand side and right-hand side of each box in (a) and (b): $a = 1$ μm and $a = 2.6$ mm, and in (c): $r = 10^{-3}$ and 10 μm, respectively.

aerosol mass inside the cloud water (curve 6), the cumulative mass of aerosol deposited on the ground by rain (curve 7), and the cumulative mass of aerosol scavenged by impaction (curve 8) are plotted as a function of time. Curve 4 decreases very slightly with time as particles are consumed by the drops, and as these are subsequently deposited on the ground. Nucleation scavenging (curve 5) begins at the onset of cloud formation, i.e. about 26 minutes after the onset of solar heating. This time correlates with the time when aerosol is first found in the cloud water (curve 6). The amount of aerosol mass removed by impaction scavenging (curve 8) is considerably smaller than that removed by nucleation. It remains insignificant until 39 minutes after the initiation of heating when precipitation size drops start leaving the cloud base. This is a result of the fact that *inside* the cloud the main aerosol mass is consumed by the nucleation of drops on the large aerosol particles, leaving to impaction scavenging only a negligible mass of small drop–interstitial aerosol particles. The effects of impaction scavenging become noticeable as soon as rain drops leave cloud base and fall through air where there are still numerous large aerosol particles. Aerosol particles scavenged by both nucleation and impaction reach the ground inside the rain shortly thereafter (curve 7). The sum of curves (5) and (8) gives the cumulative scavenged aerosol mass. This sum is larger than the sum of curves (6) and (7). The difference between these sums is due to the fact that some drops had evaporated and released the scavenged aerosol mass back into the air.

The curves given in Figs. 11 and 12 are further compared in Table 2 in terms of five efficiencies, defined as

$$E_1 \equiv \frac{\text{cumulative rain mass on the ground}}{\text{total liquid water in the domain}} = \frac{\text{curve}(3)}{\text{curves}(3) + (2)}$$

$$E_2 \equiv \frac{\text{cumulative rain mass on the ground}}{\text{cumulative water mass converted from vapor}} = \frac{\text{curve}(3)}{\text{curve}(1)}$$

$$E_3 \equiv \frac{\text{cumulative aerosol particle mass in rain}}{\text{total aerosol particle mass in the drops}} = \frac{\text{curve}(7)}{\text{curves}(6) + (7)}$$

$$E_4 \equiv \frac{\text{cumulative aerosol particle mass in rain}}{\text{cumulative aerosol mass scavenged by nucleation}} = \frac{\text{curve}(7)}{\text{curve}(5)}$$

$$E_5 \equiv \frac{\text{cumulative aerosol particle mass in rain}}{\text{cumulative aerosol mass scavenged by nucleation and impaction}} = \frac{\text{curve}(5)}{\text{curves}(5) + (8)}, \qquad (28)$$

Here E_1 and E_2 define two precipitation efficiencies with which the water vapor and the cloud water is con-

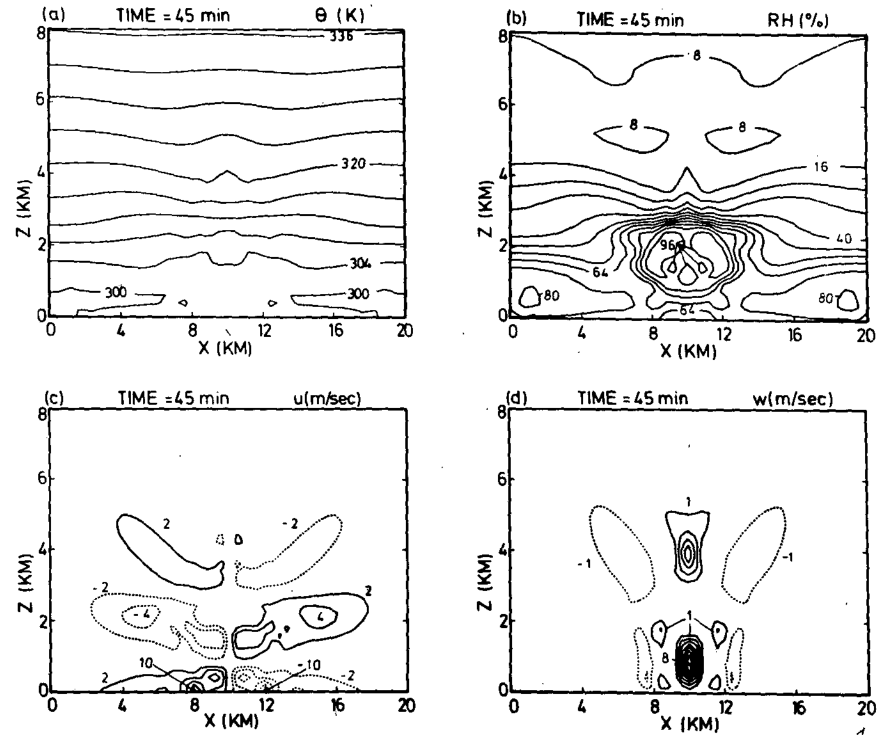

FIG. 7. Distribution of (a) θ, (b) RH, (c) u, and (d) w inside domain at $t = 45$ minutes; $\Delta\theta = 4°\text{K}$, $\Delta RH = 8\%$, $\Delta u = 2\ \text{m s}^{-1}$, $\Delta w = 1\ \text{m s}^{-1}$.

verted to rain water. The definition of these efficiencies have been chosen in a slightly different manner from those typically found in literature (e.g., see Foote and Fankhauser 1973), in order to meaningfully compare them with E_3, E_4 and E_5 for aerosol particle scavenging. The values of E_1 and E_2 show that the precipitation efficiency of the model cloud is relatively small. This is somewhat expected since the cloud is relatively shal-

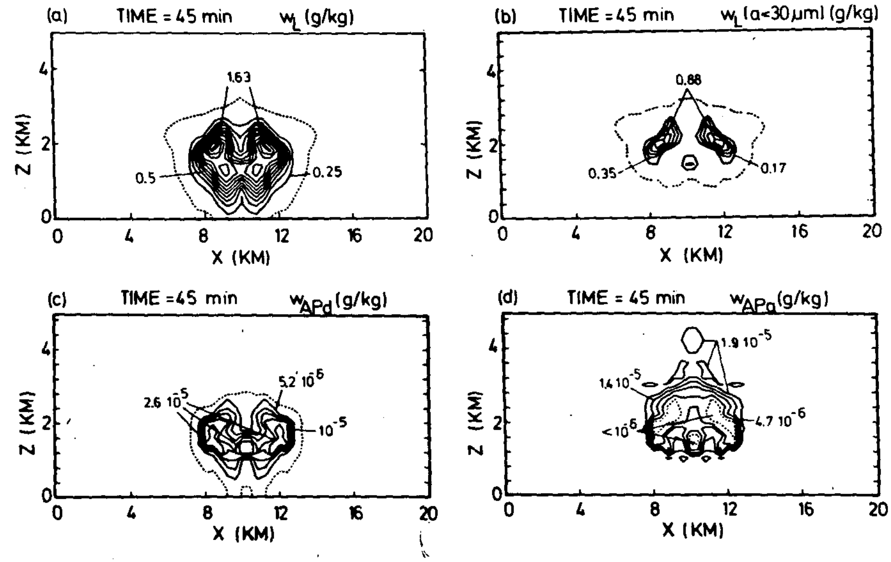

FIG. 8. Distribution of (a) w_L, (b) w_L for drops of $a < 30\ \mu\text{m}$, (c) $w_{\text{AP}d}$, and (d) $w_{\text{AP}a}$ inside domain at $t = 45$ min; $\Delta w_L = 0.125\ \text{g kg}^{-1}$, $\Delta w_L\ (a < 30\ \mu\text{m}) = 0.175\ \text{g kg}^{-1}$, $\Delta w_{\text{AP}d} = 5.2 \times 10^{-6}\ \text{g kg}^{-1}$, $\Delta w_{\text{AP}a} = 4.7 \times 10^{-6}\ \text{g kg}^{-1}$.

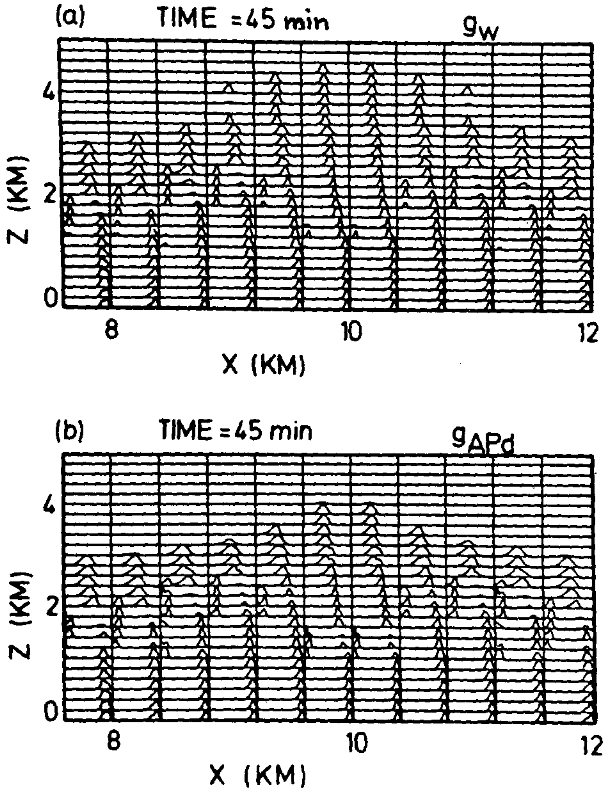

FIG. 9. Distribution of (a) g_w, (b) g_{APd} inside domain at $t = 45$ min; on the left-hand side and right-hand side of each box in (a) and (b): $a = 1$ μm and $a = 2.6$ mm, respectively.

low, subjected to considerable evaporation, and has only the relatively inefficient collision–coalescence mechanism for forming precipitation. An analogous behavior is found for the efficiencies E_3, E_4 and E_5. The close correspondence between the efficiencies E_1 and E_3 and between E_2 and E_4, or E_5 demonstrate again, in another way, that the main aerosol mass closely follows the main water mass. Efficiency E_1 will become 1 eventually, when the cloud completely evaporates and the liquid water suspended goes to zero. The same is true for E_3. In our case, however, the cloud simulation was stopped at 60 minutes when the rain stopped but the cloud had not yet completely dissipated. Efficiencies 2, 4 and 5 decrease after a maximum near 57 minutes due to the fact that deposition becomes rapidly less than the still ongoing condensation and scavenging.

Some additional conclusions can be deduced from Fig. 12. Since *impaction* scavenging contributes only negligibly to *in-cloud* scavenging but is the only *below-cloud* scavenging mechanism, it is feasible to make a comparison between *in-cloud* and *below-cloud* scavenging. Comparing the cumulative aerosol mass taken up by impaction scavenging (curve 8, Fig. 12) with the cumulative mass of aerosol taken up by both nucleation and impaction scavenging (curves 5 and 8, Fig. 12) shows that *below-cloud* scavenging only contributes about 5% to the *overall particle scavenging.* This relatively small value is due to the very low cloud base which our maritime cloud exhibited. Looking at E_5 of Table 2 we see that due to the low rain efficiency E_2, only 14% of the total scavenged aerosol mass was deposited by rain on the ground. From a comparison of curves 7 and 8 in Fig. 12 we see that *below-cloud scavenging* contributed about 40% to the aerosol mass in the rain water on the ground, assuming that all the aerosol mass which is scavenged below cloud base does reach the ground in the rain. This implies that *in-cloud*

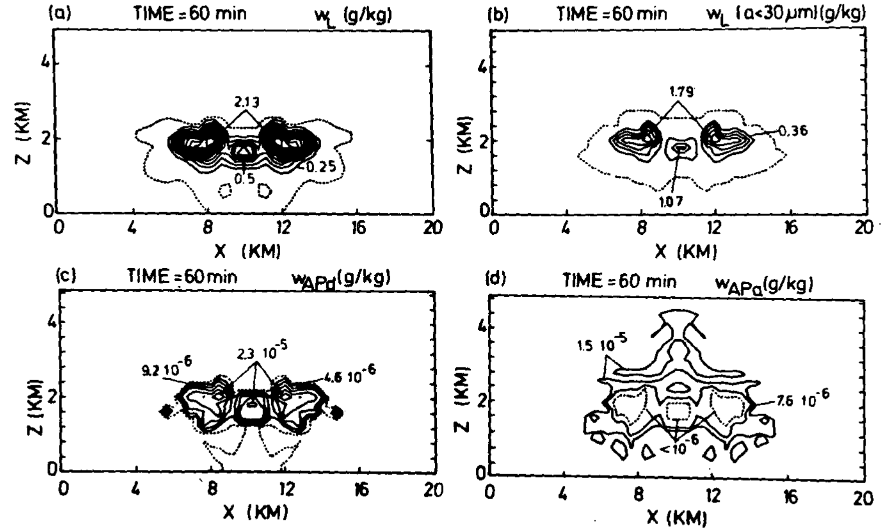

FIG. 10. Distribution of (a) w_L, (b) w_L for drops of $a < 30$ μm, (c) w_{APd}, and (d) w_{APa} inside domain at $t = 60$ min; $\Delta w_L = 0.125$ g kg^{-1}, Δw_L ($a < 30$ μm) $= 0.358$ g kg^{-1}, $\Delta w_{APd} = 4.6 \times 10^{-6}$ g kg^{-1}, $\Delta w_{APa} = 7.6 \times 10^{-6}$ g kg^{-1}.

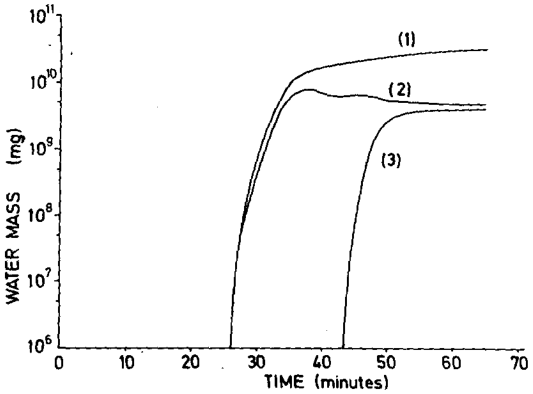

FIG. 11. Cumulative condensed water mass (curve 1), total water mass as drops in air (curve 2), and cumulative water mass as rain on the ground (curve 3), as a function of time.

TABLE 2. Precipitation and scavenging efficiencies as defined by Eq. (28) as a function of time.

Time (min)	Efficiency (%)				
	E_1	E_3	E_2	E_4	E_5
43.4	0.02	0.01	0.00	0.00	0.00
45.1	1.18	0.79	0.38	0.27	0.26
46.8	8.17	5.63	2.63	1.95	1.85
48.4	22.56	20.40	7.31	7.21	6.78
50.1	33.31	31.67	11.06	11.79	11.09
51.8	37.35	37.38	12.32	13.88	13.05
53.4	39.26	39.44	12.89	14.98	14.10
55.1	35.33	42.23	13.20	16.00	15.07
56.8	42.14	44.50	13.34	16.57	15.62
58.4	43.24	44.80	13.24	16.31	15.41
60.1	43.86	45.93	13.11	15.88	15.03
61.8	43.39	46.30	12.67	15.32	14.53
63.4	43.17	47.39	12.26	14.77	14.04

scavenging contributed about 60% to the aerosol mass in the rain on the ground.

Murakami et al. (1983) found during field observations in Japan that, for sulfate particles, below-cloud scavenging contributed to the total precipitation scavenging about 20% while Petrenchuk (1970) deduced a value of about 75% and Scott (1978) a value of about 2% to 10%. This variability is understandable if we consider that the contribution of below-cloud scavenging strongly depends on the precipitation efficiency of a cloud.

Some additional results of our computation are summarized in Table 3 and Fig. 13. In Table 3 the total rain R (column 2), the rain rate RR (column 3), the total amount of sulfur S_{dep} deposited on unit area (column 4) the deposition rate of sulfur SR_{dep} (column 5), the cumulative concentration of sulfur in the deposited rain water C_{cum} (column 6), and the concentration of sulfur in sequential rain water samples C_{seq} (column 7) have been listed for different times, and were totaled over the whole rain area. The RR, SR_{dep} and C_{seq} are sampled over 100 second intervals. Columns 2 and 3 show that the cloud system was weak in that it produced not quite 1 mm of rain, with a rain rate maximum of about 9.6 mm h^{-1} at 48 minutes. From a comparison of columns 3 and 5 we notice that the rain rate RR and the sulfur deposition rate SR_{dep} behave analogously going through a maximum at about 48 min. This again reflects the fact that the main sulfur mass is associated with the main water mass, as stated earlier. A look at the sulfur concentrations of the sequential rain water samples shows that the concentra-

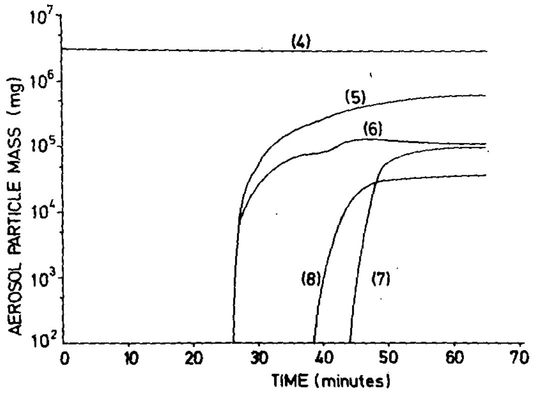

FIG. 12. Total aerosol mass in air inside computational domain (curve 4), cumulative aerosol mass scavenged by nucleation (curve 5), total aerosol mass in airborne cloud water (curve 6), cumulative aerosol mass in rain on ground (curve 7), and cumulative aerosol mass scavenged by impaction scavenging (curve 8), as a function of time.

TABLE 3. Total rain R (mm), cumulative (column 2); rain rate RR (mm h^{-1}) (column 3); total sulfur S_{dep} (mg m^{-2}), cumulative (column 4); deposition rate of sulfur SR_{dep} (mg m^{-2} h^{-1}) (column 5); concentration of sulfur in rain C_{cum} (mg liter^{-1}), cumulative (column 6); concentration of sulfur in rain C_{seq} (mg l^{-1}), sequentially sampled at time (column 7); at different times, and totalized over the whole rain area. RR, SR_{dep} and C_{seq} are sampled over 100 sec intervals.

Time (min)	R	RR	S_{dep}	SR_{dep}	C_{cum}	C_{seq}
43.4	3×10^{-4}	0.20	8×10^{-5}	0.06	0.27	0.29
45.1	0.02	1.85	0.01	0.50	0.32	0.27
46.8	0.12	6.31	0.04	2.95	0.35	0.47
48.4	0.37	9.55	0.17	5.27	0.46	0.55
50.1	0.58	5.27	0.30	3.33	0.51	0.63
51.8	0.68	2.73	0.37	2.02	0.53	0.74
53.4	0.74	1.81	0.42	1.70	0.56	0.94
55.1	0.79	1.19	0.46	1.39	0.59	1.17
56.8	0.81	0.60	0.49	0.81	0.61	1.36
58.4	0.82	0.27	0.51	0.43	0.62	1.56
60.1	0.83	0.14	0.52	0.24	0.62	1.76
61.8	0.83	0.06	0.52	0.11	0.63	1.88
63.4	0.83	0.02	0.52	0.05	0.63	2.26

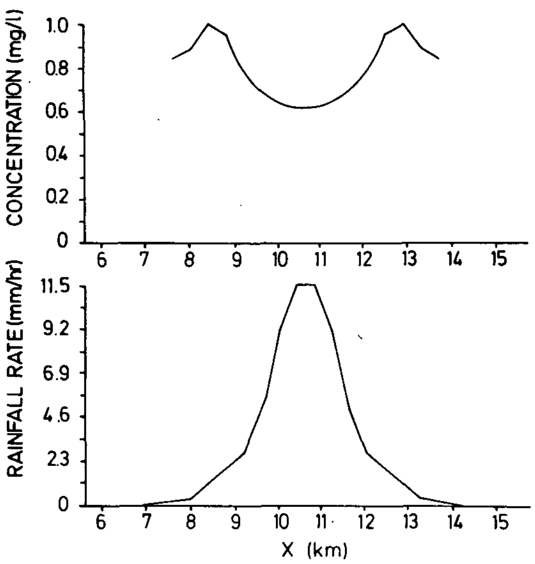

FIG. 13. Comparison of concentration of sulfur in rain water with rainfall rate across domain at $t = 50$ minutes.

tion ranges between 0.27 and 2.26 mg l^{-1}, equivalent to a sulfate concentration ranging between 0.81 and 6.78 mg l^{-1}. Unfortunately, no field measurements of the sulfur concentration in the cloud and rain water of Hawaii are available for the exact time period to which our model calculations apply. However, we never intended to describe the local cloud and precipitation chemistry of Hawaii in detail, but rather qualify some general scavenging behavior of atmospheric clouds (see our discussion in section 2). Nevertheless, we decided to check whether the computed sulfur concentrations were in line with measurements of SO_4^{2-} concentrations in rainwater collected in Hawaii. Thus, Miller and Yoshinaga (1981) measured SO_4^{2-} concentrations of 0.3 to 8.0 mg l^{-1}, Parungo et al. (1982) measured 9.6 to 38.4 mg l^{-1}, and Harding and Miller (1982) found 0.2 to 36 mg l^{-1}. Considering that our model does not yet include the contribution of gas scavenging to the SO_4^{2-} concentration, we can conclude that our model results are in line with observations.

As far as the time and spatial variation of the sulfur concentration in rain water and its relation to the precipitation rate is concerned, it was noticed during field observations (e.g., see Kins 1982) that the sulfur concentration is high in the beginning of the rain event, decreases with increasing rain rate to a maximum, and increases again towards the end of the rain event. Such behavior is reasonable, because in the beginning of the rain event the falling drops evaporate, thus raising the moisture level of the air between the cloud base and the ground and raising the sulfur concentration in the falling drops. This effect decreases rapidly as the rain rate increases, thus decreasing the sulfur concentration in the rain water. Subsequently, the concentration rises again as the cloud disintegrates and the rain rate decreases.

The results of our computations are consistent with such an observed behavior, as demonstrated in Fig. 13. This figure exhibits the rainfall rate and the sulfur concentration in the rain water across the rain domain 7 minutes after the rain first reached the ground (50 minutes after starting the simulation). This figure shows that a pronounced minimum in the sulfur concentration of the rain water is associated with a rain rate maximum underneath the cloud core, flanked by two maxima in the sulfur concentration of the rain water coming from the wings of the cloud where the rain rate is small. Would such a system pass overhead at a fixed location, it would lead to the observed rainfall rate versus concentration behavior, as seen in field observations.

Column 7 (C_{seq}) in Table 3 appears not to be in support of this behavior, as the sulfur concentration of the sequential rainfall samples is relatively low at the beginning of the rain event and steadily increases until the end of the simulation without showing a minimum at the time of the rainfall rate maximum. This behavior is the result of a masking effect caused by the fact that the values listed in column 7 are totaled over the whole rain area. Due to the very low base of the cloud considered, and the high relative humidity of the air between cloud base and ground, the falling rain drops evaporate very little during their fall, thus preventing an initial maximum of the sulfur concentration. Since the cloud system is relatively weak, it begins to deteriorate by evaporation rather quickly after the onset of rain (see Fig. 8). As a result, the sulfur concentration of the rain water, totaled over the whole rainfall domain, continues to increase even through the time of the rainfall rate maximum, as the rain with relatively high sulfur concentrations from the deteriorating cloud regions overshadows the rain of low sulfur concentration from other cloud portions.

Finally, we noticed during our model computations that the sulfur concentration varies significantly across the drop size spectrum. This implies that cloud and rain water do not have the same composition. This result is in contrast to many scavenging models less detailed than ours, particularly models with Kessler-type parameterizations (see our summary of other models in section 1).

Another quantity which has been introduced in the literature as a measure of the amount of pollutants scavenged by clouds and rain is the washout coefficient W (e.g., see Scott 1981), which is commonly defined by the ratio of the pollutant concentration in the rain water (g (pollutant/l) to the pollutant concentration in air [g(pollutant)/m^3]. In our calculations we obtain washout ratio which have values near 1000.

6. Summary and conclusions

By means of a detailed microphysical model imbedded in a two-dimensional convective cloud model, we were able to simulate the wet deposition of atmospheric aerosol particles, keeping track of the aerosol mass in the air, inside the drops in the cloud, and inside the drops which have arrived on the ground. This study of a shallow warm cumulus allows the following conclusions.

1) The collision–coalescence process caused a redistribution of the aerosol particle mass scavenged by the cloud drops in such a way that the main aerosol mass scavenged was always associated with the main water mass.

2) *Inside the cloud* scavenging of aerosol particles was almost completely controlled by nucleation scavenging.

3) The amount of sulfur removed by *below-cloud scavenging,* which is caused by impaction scavenging, contributed about 5% to the *overall particle* scavenging and contributed about 40% to the aerosol mass in the rain on the ground.

4) Due to the low rain efficiency of the cloud, only 14% of the total scavenged aerosol mass was deposited by rain on the ground.

5) Inside a cloud, a "drop-interstitial" aerosol exists which consists of small particles whose mass mixing ratio is reduced by several orders of magnitude in comparison to its value outside the cloud, i.e., nucleation scavenging removes more than 99% of the aerosol mass.

6) Contrary to the assumption made in many contemporary cloud models which include wet deposition, our results show that cloud and precipitation water do not have the same composition.

7) The sulfur concentrations in the rain water agreed reasonably well with field observations cited in literature, if consideration is given to the fact that the present calculations did not include SO_2 scavenging.

Conclusions 1, 2 and 5 meet with the expectations derived from our previous studies with a simple parcel model (Flossmann et al. 1985).

Acknowledgments. This research was funded by the Ministry for Research and Technology of the Federal Republic of Germany under Project 325-4007-070-4580. The authors of this paper are solely responsible for its content. The authors also acknowledge with gratitude the financial support of the German National Science Foundation under Project SFB 233. Both authors are deeply indebted to Drs. T. L. Clark, W. D. Hall, and G. M. Barnes of NCAR for providing access to their model for convective clouds, for having provided considerable amounts of computer time on the NCAR CRAY-1A, and for fruitful discussions. The authors also express their gratitude to Prof. P. Crutzen, Max-Planck Institute for Chemistry, for providing support for the present study.

REFERENCES

Chaumerliac, N., E. Nickerson and R. Rosset, 1983: A three dimensional mesoscale numerical simulation of atmospheric cleansing during the 1982 Boulder upslope cloud observation experiment. *Precipitation Scavenging, Dry Deposition and Resuspension,* **1,** Elsevier, 627–648.

Clark, T. L., 1977: A small scale dynamic model using a terrain-following coordinate transformation. *J. Comput. Phys.,* **24,** 186–215.

——, 1979: Numerical simulations with a three dimensional cloud model. *J. Atmos. Sci.,* **36,** 2191–2215.

——, and R. Gall, 1982: Three dimensional numerical model simulations of air flow over mountainous terrain: A comparison with observation. *Mon. Wea. Rev.,* **110,** 766–791.

——, and R. D. Farley, 1984: Severe downslope windstorm calculations in two and three spatial dimensions using anelastic interactive grid nesting. *J. Atmos. Sci.,* **41,** 329–350.

Cogbill, C. V., and G. E Likens, 1974: Acid precipitation in the northeastern United States. *Water Resour. Res.,* **10,** 1133–1137.

Darzi, M., and J. W. Winchester, 1982: Aerosol characteristics at Mauna Loa Observatory, Hawaii after East Asian dust storm episodes. *J. Geophys. Res.,* **87,** 1251–1258.

Daum, P. H., S. E. Schwartz and L. Newman, 1983: Studies of gas and aqueous phase composition of stratiform clouds. *Precipitation Scavenging, Dry Deposition and Resuspension,* **1,** Elsevier, 31–52.

Easter, R. C., and P. V. Hobbs, 1974: The formation of sulfates and the enhancement of cloud condensation nuclei in clouds. *J. Atmos. Sci.,* **31,** 1586–1594.

——, and J. M. Hales, 1983: Interpretations of the Oscar data for reactive gas scavenging. *Precipitation Scavenging, Dry Depositions and Resuspension,* **1,** Elsevier, 649–660.

Fischer, B. E. A., 1982: The transport and removal of sulfur dioxide in rain system. *Atmos. Environ.,* **16,** 775–783.

Flossmann, A. I., 1987: A theoretical investigation of the removal of atmospheric trace constituents by means of a dynamic model. Ph.D. thesis, Meteor. Institute, Joh. Gutenberg Universität. [Available from University of Mainz.]

——, W. D. Hall and H. R. Pruppacher, 1985: A theoretical study of the wet removal of atmospheric pollutants. Part I: The redistribution of aerosol particles captured through nucleation and impaction scavenging by growing cloud drops. *J. Atmos. Sci.,* **42,** 582–606.

——, H. R. Pruppacher and J. H. Topalian, 1987: A theoretical study of the wet removal of atmospheric pollutants. Part II: The uptake and redistribution of $(NH_4)_2SO_4$ particles and SO_2 gas simultaneously scavenged by growing cloud drops. *J. Atmos. Sci.,* **44,** 2912–2923.

Foote, G. B., and J. C. Fankhauser, 1973: Airflow and moisture beneath a northeast Colorado hailstorm. *J. Appl. Meteor.,* **12,** 1330–1353.

Galloway, J. N., G. E. Likens and E. S. Edgeston, 1976: Acid precipitation in the northeastern United States: pH and acidity. *Science,* **194,** 722–724.

Hales, J., 1982: Mechanistic analysis of precipitation scavenging using a one dimensional time variant model. *Atmos. Environ.,* **16,** 1775–1783.

Hall, W. D., 1980: A detailed microphysical model within a two-dimensional dynamic framework: Model description and preliminary results. *J. Atmos. Sci.,* **37,** 2486–1507.

Harding, D., and J. M. Miller, 1982: The influence of rain chemistry of the Hawaiian Volcano Kilanea. *J. Geophys. Res.,* **87,** 1225–1230.

Hegg, D. A., and P. V. Hobbs, 1982: Measurements of the sulfate production in natural clouds. *Atmos. Environ.*, **16,** 2663–2668.

——, S. A. Rutledge and P. V. Hobbs, 1984: A numerical model for sulfur chemistry in warm frontal rainbands. *J. Geophys. Res.*, **89,** 7133–7147.

Kins, L., 1982: The variation of chemical composition of rainwater during individual precipitation events. *Deposition of Atmospheric Pollutants,* Reidel, 87–96.

Lazrus, A. L., P. L. Haagenson, G. L. Koh, C. W. Huebert, K. C. W. Krietzberg, G. E. Likens, U. A. Mohnen, W. E. Wilson and J. W. Winchester, 1983: Acidity in air and water in the case of warm-frontal precipitation. *Atmos. Environ.*, **17,** 581–592.

Leaitch, W. R., J. W. Strapp, H. A. Wiebe and G. A. Isaac, 1983: Measurements of scavenging and transformation of aerosol inside cumulus. *Precipitation Scavenging, Dry Deposition and Resuspension,* **1,** Elsevier, 53–70.

Lilly, D. K., 1962: On the numerical simulation of buoyant convection. *Tellus,* **14,** 148–172.

Miller, J. M., and A. M. Yoshinaga, 1981: The pH of Hawaiian precipitation, a preliminary report. *Geophys. Res. Lett.*, **8,** 779–782.

Molenkamp, C. R., 1983: A scavenging model for stratified precipitation. *Precipitation Scavenging, Dry Deposition and Resuspension,* **1,** Elsevier, 597–608.

Murakami, M., T. Kimura, C. Magono and K. Kikuchi, 1983: Observations of precipitation scavenging for water soluble particles. *J. Meteor. Soc. Japan,* **61,** 346–357.

Ohta, S., T. Okita and C. Kato, 1981: A numerical model of acidification of cloud water. *J. Meteor. Soc. Japan,* **59,** 892–901.

Orville, H. D., 1965: A numerical study of the initiation of cumulus clouds over mountainous terrain. *J. Atmos. Sci.*, **24,** 648–699.

Paluch, I. R., 1979: The entrainment mechanism in Colorado cumuli. *J. Atmos. Sci.*, **36,** 2467–2478.

Parungo, F., C. Nagamoto, I. Nolt, M. Dias and E. Nickerson, 1982: Chemical analysis of cloud water collected over Hawaii. *J. Geophys. Res.*, **87,** 8805–8810.

Petrenchuk, O. P., and E. S. Seleznera, 1970: Chemical composition of precipitation in regions of the Soviet Union. *J. Geophys. Res.*, **75,** 3627–3634.

Radke, L., 1983: Preliminary measurements of the size distribution cloud interstitial aerosol. *Precipitation Scavenging, Dry Deposition and Resuspension,* **1,** Elsevier, 71–78.

Richards, L. W., J. A. Anderson, D. L. Blumenthal, J. A. McDonald, G. L. Kok and A. L. Lazrus, 1983: Hydrogen peroxide and sulfur (IV) in Los Angeles cloud water. *Atmos. Environ.*, **17,** 911–914.

Rodhe, H., 1978: Budgets and turn over times of atmospheric sulfur compounds. *Atmos. Environ.*, **12,** 671–680.

——, 1983: Precipitation scavenging and tropospheric mixing. *Precipitation Scavenging, Dry Deposition and Resuspension,* **1,** Elsevier, 719–729.

Rutledge, S. A., and P. V. Hobbs, 1983: The mesoscale and microscale structure and organization of clouds and precipitation in midlatitude cyclones. VIII: A model for the seeder-feeder process in warm frontal rainbands. *J. Atmos. Sci.*, **40,** 1185–1206.

Sarma, R. A., 1983: Distribution of acidity in collective clouds due to the aqueous phase oxidation of sulfur dioxide by ozone—a numerical simulation. *Precipitation Scavenging, Dry Deposition and Resuspension,* **1,** Elsevier, 617–626.

Scott, B. C., 1978: Parameterization of sulfate removal by precipitation. *J. Appl. Meteor.*, **17,** 1375–1389.

——, 1981: Sulfate washout ratios in winter storms. *J. Appl. Meteor.*, **20,** 619–625.

——, 1982: Predictions of in-cloud conversion rates of SO_2 and SO_4 based on a single chemical and kinetic storm model. *Atmos. Environ.*, **16,** 1735–1752.

Smagorinsky, J., 1963: General circulation experiments with the primitive equations: 1. Basic experiment. *Mon. Wea. Rev.*, **91,** 99–164.

Smolarkiewicz, P. K., and T. L. Clark, 1985: Numerical simulation of the evolution of a three dimensional field of cumulus clouds. Part I: Model description, comparison with observations and sensitivity studies. *J. Atmos. Sci.*, **42,** 502–522.

Trembley, A., and H. Leighton, 1984: The influence of cloud dynamics upon the redistribution and transformation of atmospheric SO_2—a numerical simulation. *Atmos. Environ.*, **18,** 1885–1894.

Walcek, C. J., and G. R. Taylor, 1986: A theoretical method for computing vertical distributions of acidity and sulfate production within cumulus clouds. *J. Atmos. Sci.*, **43,** 339–355.

Yau, M. K., 1980: The effects of evaporation, water load and wind on cloud development in a three dimensional numerical model. *J. Atmos. Sci.*, **37,** 488–494.